Published in final edited form as:
Nano Lett. 2011 July 13; 11(7): 2678–2683. doi:10.1021/nl200858y.

Nanomaterials for X-ray Imaging: Gold Nanoparticle-Enhancement of X-ray Scatter Imaging of Hepatocellular Carcinoma

Danielle Rand[1], **Vivian Ortiz**[2], **Yanan Liu**[1], **Zoltan Derdak**[2], **Jack R. Wands**[2], **Milan Tatíček**[3], and **Christoph Rose-Petruck**[1]

[1] Department of Chemistry, Brown University, Providence, RI 02912

[2] The Liver Research Center, Rhode Island Hospital and Warren Alpert Medical School of Brown University

[3] Faculty of Biomedical Engineering, Czech Technical University, Prague, Czech Republic

Abstract

We present the development of a new imaging technique for the early diagnosis of hepatocellular carcinoma that utilizes surface-modified gold nanoparticles in combination with x-ray imaging. Tissues labeled with these electron-dense particles show enhanced x-ray scattering over normal tissues, distinguishing cells containing gold nanoparticles from cells without gold in x-ray scatter images. Our results suggest that this novel approach could enable the *in vivo* detection of tumors as small as a few millimeters in size.

Keywords

Gold nanoparticles; x-ray scattering; spatial harmonic imaging; layer-by-layer assembly; hepatocellular carcinoma; early diagnosis

Hepatocellular carcinoma (HCC) is the most common form of liver cancer in adults, accounting for approximately 3 out of every 4 cancers that start in the liver.[1] According to the most recent estimates by the American Cancer Society, over 24,000 new cases of primary liver cancer develop each year in the United States, and approximately 19,000 of these cases result in death. HCC is also especially common in developing countries, particularly in sub-Saharan Africa and Southeast Asia.[2,3] Overall, more than 500,000 people are diagnosed with this disease each year worldwide.[2,4]

Unfortunately, HCC is difficult to diagnose in its earliest stages because there are no screening tests available, and it usually only becomes symptomatic when the tumor reaches approximately 4.5–8 cm in diameter.[2,5] Current methods of detection include ultrasound examination and imaging by CT scan or MRI, but each of these methods has inherent problems, and definitive diagnosis of HCC by these modalities has proven elusive.[4,6,7] In particular, the sensitivity of these techniques continues to be problematic, making the detection of early tumors (smaller than a few centimeters in diameter) difficult.[2,5,7,8] Problems with specificity can also lead to misdiagnosis and false positive or false negative results.[5–8] Together, these difficulties contribute to the poor prognosis of HCC: the American Cancer Society estimates a 5-year survival rate of just 10%.

Correspondence to: Christoph Rose-Petruck.

The development of new techniques for the imaging and early diagnosis of HCC and other cancers is therefore crucial to improving the prognosis of these diseases, and nanotechnology has recently emerged as a field that could offer a number of promising solutions. Here we discuss the development of a new imaging technique that utilizes gold nanoparticles coated with a bilayer of polyelectrolyte. When these biocompatible nanoconstructs are taken up by cells via phagocytosis, they scatter incident x-radiation in detectable amounts, giving an enhanced signal in x-ray scatter images over that measured for cells containing no gold. We show here that x-ray scatter imaging can be more sensitive than typical absorption-based x-ray imaging.

Gold nanoparticles have been studied previously as potential contrast agents for x-ray imaging; they are good candidates because they are nontoxic and have a higher atomic number and x-ray absorption coefficient than typical iodine-based contrast agents.[9–11] For instance, Hainfeld et al. found that the biodistribution of small gold nanoparticles injected intravenously can be detected by x-ray imaging.[9] Similarly, Kim et al. have shown that gold nanoparticles approximately 30 nm in diameter can be injected intravenously and used for *in vivo* computed tomography (CT) imaging, specifically of hepatoma in the liver.[10] In both of these cases, however, successful imaging required the *in vivo* injection of large quantities of gold. We believe that the enhanced sensitivity of the x-ray scatter imaging technique proposed here over that of typical absorption based x-ray imaging could reduce the amount of gold required for visible contrast. Additionally, because scattered x-radiation can be very well separated from transmitted radiation due to the different angles at which they reach the detector, our scatter technique could lead to nearly background-free imaging.

As shown in this study, x-ray scatter imaging has the potential to detect tumors significantly below current detection limits; namely, when they are just a few millimeters in size. It is also a versatile technique that could be applied to the imaging and diagnosis of a number of different types of cancers and other systems that contain nanoparticles. To our knowledge, this is the first study that uses metal nanoparticles as agents to enhance x-ray scattering signal for the imaging of tumor-like masses.

All chemicals were purchased from Sigma (Sigma-Aldrich, St. Louis, MO) unless otherwise specified. Uncoated gold nanoparticles (10 nm and 50 nm diameter) stabilized by citrate buffer were purchased from British Biocell International (Cardiff, UK). The uptake of the nanoparticles by cancer cells is enhanced by coating the gold surfaces with two layers of polyelectrolytes (see Figure 1). The anionic poly(acrylic acid) (PAA) is deposited first, leaving carboxylic acid groups on the nanoparticle surface; this layer is followed by the cationic poly(allylamine hydrochloride) (PAH), which adds amine groups to the nanoparticle surface. The layer-by-layer (LBL) assembly of these polyelectrolytes on the gold surface relies on electrostatic interactions between the oppositely charged layers.

Stock solutions of PAA and PAH were prepared at 10 mg/mL in 1 mM aqueous NaCl solution. 1 mL aliquots of the as-purchased, unpurified gold nanoparticles were mixed with 100 μL of 1 mM NaCl and 200 μL of PAA. After 30 min adsorption time, excess polymer in the supernatant was removed by centrifugation, and nanoparticle pellets were resuspended in 1X phosphate buffered saline (PBS) solution. The procedure was then repeated using PAH, producing gold nanoparticles coated with an inner layer of PAA and an outer layer of PAH. Coated nanoparticle solutions were stored at room temperature.

Layer-by-layer coating with polyelectrolytes has been identified as a simple, versatile method for modifying the surface chemistry of nanoscale materials including gold nanoparticles and nanorods.[12–14] These types of coatings are particularly useful in that the charged polyelectrolytes can act to stabilize colloidal suspensions. Furthermore, the

thickness of the polyelectrolyte coating is easily controlled by tuning the number of layers deposited on the surface in question.[12,13] It is also possible to present specific functional groups on the nanoparticle surface simply by changing the polyelectrolytes used, enabling these coatings to act as platforms for further functionalization of the nanoparticle.[14]

PAA/PAH polyelectrolyte coatings have previously been shown to make surfaces cell adhesive when deposited under certain pH conditions.[15] Because PAA and PAH are weak polyelectrolytes, their degrees of ionization (and therefore the strength of the electrostatic interactions between them) are pH-dependent.[16] The PAA and PAH stock solutions used here have a pH of 8.4 and 3.7, respectively, and under these conditions, PAA (pKa ~ 4.5) and PAH (pKa ~ 8.5) are both essentially fully charged. Anionic, deprotonated carboxylic acid groups on PAA interact strongly with cationic, protonated amine groups on PAH, bringing the oppositely charged layers close together and producing thin, flat coatings on the nanoparticle surface. Because the alternating polyelectrolyte layers are so tightly crosslinked by these ionic interactions, water is unable to penetrate this surface layer; the coated nanoparticles therefore present very hydrophobic surfaces to their surrounding environment. This hydrophobicity has been shown to translate to cytophilicity[17–19], suggesting that the polyelectrolyte-coated nanoparticles used here will easily be taken up by cells via phagocytosis.

Phagocytosis of the 10 nm and 50 nm PAA-PAH coated gold nanoparticles by living cells was examined using a human hepatocellular carcinoma cell line (FOCUS).[20] FOCUS cells are a good model for the study of targeted cancer therapy due to the presence of specific antigens on the FOCUS cell surface that can be recognized by monoclonal antibodies.[21–24] Cancerous cells such as these can be targeted *in vivo* by monoclonal antibodies that bind to tumor-associated antigens, delivering imaging or therapeutic agents to the targeted cells while avoiding uptake by healthy cells. For example, it has been shown that the monoclonal antibody FB50 can be used as a biomarker for HCC due to a strong antibody-antigen interaction between FB50 and aspartyl (asparaginyl)-β-hydroxylase, a protein overexpressed in liver cancer cells.[24] Although no specific targeting of the cells by the gold nanoparticles is required here, the FOCUS cell line was chosen so that these features may be taken advantage of in future studies.

FOCUS cells were maintained at 37°C in an atmosphere of 5% CO_2 in Eagle's Minimum Essential Medium (EMEM) supplemented with 10% fetal bovine serum, 1% penicillin/streptomycin and 1% L-glutamine. Upon confluency, cells were detached using trypsin and resuspended in serum-free EMEM. Cells were counted, separated into pellets of equal size (approximately 10^7 FOCUS cells per pellet), and incubated with nanoparticle solutions of varying gold concentrations for 1 h at 37°C. The size of the pellet was chosen to imitate the size of a small tumor. After incubation, the cells were washed three times with PBS to remove any excess gold in the supernatant and resuspended in serum-free medium for imaging.

The *in vitro* uptake of the gold nanoparticles used in this study by the FOCUS HCC cell line is limited when the nanoparticles are not coated with polyelectrolyte; on average, less than 25% of the uncoated nanoparticles used for incubation are taken up by the FOCUS cells over 1h incubation time. Potential signal enhancements in x-ray scatter images are therefore reduced due to the low gold concentrations in each cell (see Table 1). However, wrapping the nanoparticles in the cytophilic PAA/PAH coating discussed above enhances their phagocytosis by the FOCUS cells, increasing the amount of gold in each cell and therefore the potential scattering signal seen when x-ray images are taken. When equal amounts of polyelectrolyte-coated and uncoated gold are incubated with FOCUS cells under the same

conditions, the cells phagocytose more than twice as much PAA/PAH coated gold as they do uncoated gold (Table 1).

Assembling PAA and PAH in a layer-by-layer fashion on our 10 nm and 50 nm gold nanoparticles therefore enables us to reliably test our imaging technique, as the nanoparticles are taken up into living HCC cells in higher amounts. It is interesting to note that this uptake is not dictated by the number of gold nanoparticles interacting with each cell: although in these studies individual FOCUS cells take up approximately 275,000 polyelectrolyte-coated 10 nm gold nanoparticles, they phagocytose an average of only 2000 polyelectrolyte-coated 50 nm gold nanoparticles (Table 1). We found instead that it is the total volume of gold, rather than the number of nanoparticles, that appears to be the most important factor in determining the extent of cellular uptake. Additionally, calculated volume fractions indicate than only a very small portion of each cell is actually occupied by nanoparticles: in these studies, less than 0.001% of the volume of each cell contains gold.

To prepare samples for x-ray scatter imaging, three cell pellets containing approximately 10^7 FOCUS cells (volumes of tissues a few millimeters in diameter, resembling small tumors in size) were incubated with solutions containing 10 nm gold nanoparticles, 50 nm gold nanoparticles, or no gold. The mass of gold used for incubation was the same regardless of nanoparticle size. Furthermore, this incubation process was carried out twice using a different mass of gold each time, giving six chemically different FOCUS pellets over the two separate incubations. The four pellets that contain gold nanoparticles are distinguishable both by the mass of gold nanoparticles present in the cells (slightly higher for the second incubation) and the size of the nanoparticles used (10 nm versus 50 nm gold nanoparticles). After both incubations, the cells were collected, washed and imaged.

The imaging technique applied here, called Spatial Harmonic Imaging (SHI)[25–27], uses x-rays scattered by the sample to form an image. The deflection of incident x-rays from the primary beam direction by the sample is detected by placing an absorption grid between the sample and the x-ray camera, causing a blurring in the resulting image as shown in Figure 2. Fourier transformation of the image obtained with the grid in place converts the product of x-ray transmittances of the sample and the grid into a convolution in the spatial frequency domain (see Figure 3). The grid, a periodic structure, produces a series of peaks in this convolution, and each peak is “surrounded” by the spatial frequency spectrum of the sample.

Selecting an area around a specific peak in the convolution and Fourier back-transforming this area returns the logarithm of the scattered intensities to real space and gives a processed image that contains anisotropic information regarding how the samples scatter the incident x-rays. The area surrounding the central 0^{th}-order peak (white box in Figure 3) corresponds to the original x-ray absorption image without scatter. It can therefore be used for normalization; this image is subtracted from the higher order images to remove all absorption features. The area around the 1^{st}-order peak to the immediate left of the 0^{th}-order peak (red box in Figure 3) corresponds to scattering in the x-direction, and therefore gives a processed “left 1^{st}-order” scatter image upon Fourier back-transformation and normalization. Similarly, the area around the 1^{st}-order peak immediately above the 0^{th}-order peak (green box in Figure 3) corresponds to scattering in the y-direction, and therefore gives a processed “upper 1^{st}-order” scatter image upon Fourier back-transformation and normalization. Thus, every x-ray image taken yields two processed images; one resulting from x-radiation scattered horizontally, and another resulting from x-radiation scattered vertically. Both 1^{st} order images should measure identical scatter signals because of the isotropic scattering of the spherical nanoparticles.

The scattering signal S for each processed image is calculated according to the following equation

$$S = -\log\left(\frac{I_1/G_1}{I_0/G_0}\right), \tag{1}$$

where I_1 and I_0 are the detected x-ray signals with sample in the 1st and 0th order, respectively. G_1 and G_0 denote the detected x-ray signals without sample in the 1st and 0th order, respectively. The signal S is calculated for each vial in the area that contains the cell pellet and the area of the supernatant. We denote these signals S_{cells} and S_{super}, respectively. Care was taken not to include any signal from the vial walls. The normalized scattering signal for each cell pellet is calculated by dividing the signal measured in the area containing the cell pellet by the signal measured in the area of the supernatant:

$$S_{norm} = \frac{S_{cells}}{S_{super}}. \tag{2}$$

This normalized scattering signal is then compared to the absorbance measured in the original absorption x-ray images. The absorbance is given by

$$A = -\log\left(\frac{I_{sample}}{I_{flat\ field}}\right). \tag{3}$$

In equation 3, I_{sample} is the detected x-ray intensity with a sample vial and $I_{flat\ field}$ is the detected x-ray intensity without a sample vial. The signal A is calculated for each vial in the area containing the cell pellet and in the area of the supernatant above. We denote these signals A_{cells} and A_{super}, respectively. The normalized signal measured for each pellet in the absorption images is calculated by dividing the signal measured in the area containing the cell pellet by the signal measured in the area of the supernatant:

$$A_{norm} = \frac{A_{cells}}{A_{super}}. \tag{4}$$

Finally, scattering signal can be compared to the signal measured in the absorption images by calculating an enhancement factor:

$$Enhancement\ factor = \frac{S_{norm}}{A_{norm}}. \tag{5}$$

The measurements were done with a microfocus x-ray tube (Trufocus Corporation, model: TFX-3110EW) with a tungsten anode. The tube was operated at an electrical power of 20 W, giving a maximum voltage of 95.6 kV. High voltages are used to reduce required exposure times; they are also better suited for eventual *in vivo* applications, as imaging a tumor in a mouse model will require large penetration depths. The distance between the source and camera is 1.6 m, and the sample is placed halfway between the source and camera to enhance resolution.[26] A stainless steel absorption grid with a pitch of 50 μm was purchased from Small Parts, Inc. (Seattle, WA) and positioned directly in front of the vials.

The images were acquired with an x-ray CCD camera (Princeton Instruments, Model Quad-RO 4096). The total exposure time for each image was 180 s.

We applied SHI to the pellets of FOCUS cells containing either 10 nm gold nanoparticles, 50 nm gold nanoparticles, or no gold. Two separate incubations gave two sets of pellets, and each set of pellets was imaged three times in three different orientations in order to exclude any false signals due to possible non-uniformities of the sensitivity of the imaging system. A holder was designed to keep the vials in position while the images were taken. Holes of the same size were drilled through a thin block of aluminum so that the vials, when placed into these holes, sit at exactly the same height. Processing the absorption images as described above gives six x-ray scatter images of every pellet. Overall, there are four chemically different pellets labeled with gold nanoparticles and 6 processed images of each, giving 24 x-ray scatter images of FOCUS cells containing gold nanoparticles.

As shown in Figure 4, photos of pellets of approximately 10^7 FOCUS cells containing 50 nm gold nanoparticles, no gold, and 10 nm gold nanoparticles display gold labeling clearly. Cells containing gold are stained brown; the EMEM supernatant is naturally pink and does not indicate the presence of gold nanoparticles. In a conventional x-ray absorption image, it is impossible to distinguish between the pellets labeled with gold and the pellet containing no gold. The signal enhancement due to gold labeling seen in these absorption images (Figure 4b) is determined by taking an average intensity profile of the image at the pellet height (which should change depending on gold concentration) and normalizing it by the intensity of the supernatant (which should be the same for all three pellets). The upper and lower boxes in each image of Figure 4 indicate the areas selected for intensity profiles of the supernatant and pellet, respectively; intensity values are averaged over these selected areas. Use of the holder described above ensures that, when average signal intensities are taken in each image, comparisons between the samples are made at positions where the samples have the same thickness.

Analysis of the absorption x-ray images shows that the signal measured for cells containing gold is 1.2% greater than that measured for cells without gold (see Table 2). However, of the 12 absorption images taken of FOCUS cell pellets labeled with gold nanoparticles, only 7 exhibit any enhancement due to gold labeling. The resulting large standard deviation shows that distinctions between cells with gold and cells without gold are unreliable in absorption images, as the enhancement seen due to gold labeling is statistically insignificant.

X-ray scatter imaging, however, allows us to reliably distinguish gold-labeled cells from cells containing no gold. The left 1^{st}-order (Figure 4c) and upper 1^{st}-order (Figure 4d) scatter images give normalized pellet intensity profiles that correspond to the logarithm of the intensity of the scattered x-radiation. Both 1st order images should measure identical scatter signals because of the isotropic scattering of the spherical nanoparticles. The only differences that can be seen are the enhancement of the side interfaces with air of the vial (Figure 4c) and the bottom interface of the vial (Figure 4d). These effects are due to the anisotropic x-ray scattering at smooth material interfaces.

Analysis of these processed scatter images shows an average signal enhancement due to gold labeling that ranges from approximately 1.6% to 4.4% (Table 2). Of the 24 x-ray scatter images taken of FOCUS cell pellets labeled with gold nanoparticles, 21 show a signal enhancement when compared to x-ray scatter images of FOCUS pellets containing no gold. Overall, the data give an enhancement factor for scatter imaging (see equation 5) of greater than three.

The signal enhancement in the processed x-ray images due to increased scattering by the gold nanoparticles can be normalized by gold content in the cells. After the pellets were

imaged, the amount of gold taken up by the FOCUS cells during incubation was determined by inductively-coupled plasma atomic emission spectroscopy (ICP-AES). Samples were prepared for ICP-AES analysis by digesting gold and organics with aqua regia (1:3 mixture of HNO_3:HCl) followed by dilution in 2% nitric acid. For each pellet containing approximately 10^7 FOCUS cells, gold content ranged from 4–8 μg, corresponding to several hundred 50 nm nanoparticles per cell and tens of thousands of 10 nm nanoparticles per cell (see Table 2). Thus, for every 1 pg of gold taken up by each cell, the signal seen in the processed scatter images is enhanced by an average of 3.6% in incubation 1 and 5.7% in incubation 2. Furthermore, our studies have shown that it is possible for each cell to phagocytose an average of almost 3 pg of gold nanoparticles (see Table 1), giving a potential signal enhancement due to gold labeling of approximately 17% in logarithm scale (Table 2).

The ultimate goal of this work it to apply the x-ray scatter imaging technique *in vivo*, and to do so, the signal enhancement due to gold nanoparticle labeling must be visible beneath many layers of tissue. To mimic the thickness of tissue that the scattered x-radiation would be required to penetrate in a mouse model, x-ray images of the pellets collected from incubation 2 were also taken beneath 1 cm of water. Water and typical liver tissues have similar radiological densities, as their electron densities differ by less than 5%.[28] This is demonstrated by the lack of a visibly distinguishable boundary between the pellet and the supernatant in the x-ray images shown in this paper (see Figure 4). Similar to the results described above, x-ray scatter imaging enables the detection of gold-labeled FOCUS cell pellets even under 1 cm of water, with normalized signal intensities in the scatter images increasing by 1.8 ± 0.5% when gold nanoparticles are present in the cells.

In conclusion, our results show that pellets of HCC cells containing gold nanoparticles of different sizes can be distinguished from similar cell pellets devoid of gold *in vitro*. Over 85% of the x-ray scatter images obtained in this study show signal enhancement when comparing pellets of HCC cells labeled with gold nanoparticles to untreated HCC cells. Furthermore, based on our previous studies of the phagocytosis of PAA-PAH coated gold nanoparticles by FOCUS cells, we can predict the enhancement that should be seen due to potential gold labeling. Specifically, because we have seen that each FOCUS cell has the ability to phagocytose approximately 3 pg of gold nanoparticles, and our x-ray scatter imaging is shown here to enhance visibility by up to 5.7% for every 1 pg of gold in the cells, we predict that x-ray scatter imaging could enhance visibility of gold nanoparticle-labeled cells by over 17% on a logarithmic scale.

The cell pellets used in this experiment are several millimeters in diameter, resembling the size of a small tumor. This suggests that SHI has the potential to detect tumors that are significantly below the detection limits of current imaging techniques for HCC and many other cancers, which can often go undiagnosed until they are several centimeters in size. Signal enhancements can also be seen when the samples are placed under water, which has a similar radiological density as healthy liver tissue, indicating that the technique could be successful in an animal model. Based on our results, we believe that SHI has the potential to detect small *in situ* tumors (less than a few millimeters in size) *in vivo*.

Recently, gold nanomaterials have been used for applications in cancer therapy as well as imaging. For example, gold nanoshells have been developed for use in photothermal cancer therapy.[29–31] These nanoshells have highly tunable plasmon resonances, allowing them to absorb light strongly if the frequency of the incoming light matches their plasmon oscillation frequencies. The nanoshells can then convert energy absorbed from this light into heat, killing any cells containing nanoshells while leaving surrounding unlabeled tissue unharmed. Clinical trials of this therapy are already underway.[31] Gold nanoparticles have

also been used to provide dose enhancement in cancer radioablation therapy. Hainfeld et al. have shown that small gold nanoparticles injected intravenously can accumulate in tumors and improve x-ray therapy at the tumor site.[32] As both of the therapeutic applications discussed above use electron-dense nanomaterials, it is possible that our x-ray scatter imaging technique could be used in combination with these and similar applications for the dual imaging and therapy of various systems.

In future studies, directed targeting and imaging of tumors in an animal model could be possible through use of the cell-specific antibodies discussed above.[23,24] The amine groups presented at the surface of the gold nanoparticles by the outer polyelectrolyte layer (PAH) can be conjugated to the C-termini of an antibody by EDC/NHS crosslinking chemistry. Alternatively, the polyelectrolyte coatings could be replaced with more cell-resistant coatings to help prevent nonspecific uptake of the nanoparticles *in vivo* (specifically by macrophages in the liver). In particular, polyethylene glycol (PEG) has been shown to prevent nonspecific protein adsorption, reduce nonspecific cellular uptake, and increase the circulation times of nanoparticles in the bloodstream.[18,19,33,34] The cell-specific antibodies can then be attached to the PEGylated nanoparticle surface, again using EDC/NHS crosslinking chemistry. These nanoparticle-antibody conjugates could target specific cancers *in vivo*, delivering gold to the tumors in question and allowing them to be imaged with our proposed technique.[35,36]

The use of antibody-conjugated nanoparticle solutions, as well as longer incubations with gold solutions of higher concentrations, should result in an increased cellular uptake of gold nanoparticles. As shown in Table 1, less than 0.001% of each cell volume is occupied by nanoparticles; it seems entirely possible, therefore, that we would be able to significantly increase amount of gold in each cell, thereby increasing scatter signal and, ultimately, enhancing visibility in scatter images. Overall, the sensitivity and potential specificity of the novel nanoparticle-based imaging technique proposed here make it a promising method for the early detection and diagnosis of cancers such as HCC.

Acknowledgments

CRP acknowledges financial support for the development of the x-ray imaging modality by the U.S. Department of Energy under grant DE-FG02-08ER15937. DR acknowledges financial support by the US Department of Education through GAANN Award P200A090076, administered by the Institute for Molecular and Nanoscale Innovation at Brown University. JRW acknowledges financial support by the National Institutes of Health under grant CA123544. We thank Joseph Orchado for his technical assistance with ICP-AES measurements and Gerald Diebold for helpful discussions.

References

1. El-Sarag HB, Mason AC. The New England Journal of Medicine. 1999; 340:745–750. [PubMed: 10072408]
2. Trevisani F, Cantarini MC, Wands JR, Bernardi M. Carcinogenesis. 2008; 29:1299–1305. [PubMed: 18515282]
3. O'Brien TR, Kirk G, Zhang M. The Cancer Journal. 2004; 10:67–73. [PubMed: 15130266]
4. Bruix J, Hessheimer AJ, Forner A, Boix L, Vilana R, Llovet JM. Oncogene. 2006; 25:3848–3856. [PubMed: 16799626]
5. Colombo M. J Hepatol. 1992; 15:225–236. [PubMed: 1324273]
6. Hain SF, Fogelman I. The Cancer Journal. 2004; 10:121–127. [PubMed: 15130271]
7. Okuda K. J Hepatol. 2000; 32:225–237. [PubMed: 10728807]
8. Sheu J, Sung J, Chen D, Lai M, Wang T, Yu J, Yang P, Chuang C, Yang P, Lee C, Hsu H, How S. Cancer. 1985; 56:660–666. [PubMed: 2408739]

9. Hainfeld JF, Slatkin DN, Focella TM, Smilowitz HM. Br J Radiol. 2006; 79:248–253. [PubMed: 16498039]
10. Kim D, Park S, Lee JH, Jeong YY, Jon S. J Am Chem Soc. 2007; 129:7661–7665. [PubMed: 17530850]
11. Kojima C, Umeda Y, Ogawa M, Harada A, Magata Y, Kono K. Nanotechnology. 2010; 21:245104. [PubMed: 20498528]
12. Mayya KS, Schoeler B, Caruso F. Adv Funct Mater. 2003; 13:183–188.
13. Gittins DI, Caruso F. J Phys Chem B. 2001; 105:6846–6852.
14. Gole A, Murphy CJ. Chem Mater. 2005; 17:1325–1330.
15. Mendelsohn JD, Yang SY, Hiller JA, Hochbaum AI, Rubner MF. Biomacromolecules. 2003; 4:96–106. [PubMed: 12523853]
16. Shiratori SS, Rubner MF. Macromolecules. 2000; 33:4213–4219.
17. Lee JH, Lee HB, Andrade JD. Prog Polym Sci. 1995; 20:1043–1079.
18. Alexis F, Pridgen R, Molnar LK, Farokhzad OC. Mol Pharm. 1998; 5:505–515. [PubMed: 18672949]
19. Brandenberger C, Muhlfeld C, Zulqurnain A, Lenz A, Schmid O, Parak WJ, Gehr P, Rothen-Rutishauser B. Small. 2010; 6:1669–1678. [PubMed: 20602428]
20. He L, Isselbacher KJ, Wands JR, Goodman HM, Shih C, Quaroni A. In Vitro. 1984; 20:493–504. [PubMed: 6086498]
21. Hurwitz E, Stancoviski I, Wilchek M, Shouval D, Takahashi H, Wands JR, Sela M. Bioconjugate Chem. 1990; 1:285–290.
22. Takahashi H, Carlson R, Ozturk M, Sun S, Motte P, Strauss W, Isselbacher KJ, Wands JR, Shouval D. Gastroenterology. 1989; 96:1317–1329. [PubMed: 2703116]
23. Mohr L, Yeung A, Aloman C, Wittrup D, Wands JR. Gastroenterology. 2004; 127:S225–S231. [PubMed: 15508088]
24. Luu M, Sabo E, de la Monte SM, Greaves W, Wang J, Tavares R, Simao L, Wands JR, Resnick MB, Wang L. Hum Pathol. 2009; 40:639–644. [PubMed: 19200576]
25. Stein AF, Ilavsky J, Kopace R, Bennett EE, Wen H. Opt Express. 2010; 18:13271–13278. [PubMed: 20588456]
26. Wen H, Bennett EE, Hegedus MM, Rapacchi S. Radiology. 2009; 251:910–918. [PubMed: 19403849]
27. Wen H, Bennett EE, Hegedus MM, Carroll SC. IEEE Trans Med Imaging. 2008; 27:997–1002. [PubMed: 18672418]
28. Yang M, Virshup G, Clayton J, Zhu XR, Mohan R, Dong L. Physics in Medicine and Biology. 2010; 55:1343–1362. [PubMed: 20145291]
29. Hirsch LR, Stafford RJ, Bankson JA, Sershen SR, Rivera B, Price RE, Hazle JD, Halas NJ, West JL. Proc Natl Acad Sci USA. 2003; 100:13549–13544. [PubMed: 14597719]
30. Choi M, Stanton-Maxey K, Stanley J, Levin C, Bardhan R, Akin D, Badve S, Sturgis J, Robinson JP, Bashir R, Halas NJ, Clare S. Nano Lett. 2007; 7:3759–3765. [PubMed: 17979310]
31. Lal S, Clare SE, Halas NJ. Acc Chem Res. 2008; 41:1842–1851. [PubMed: 19053240]
32. Hainfeld JF, Slatkin DN, Smilowitz HM. Physics in Medicine and Biology. 2004; 49:N309–N315. [PubMed: 15509078]
33. Hucknall A, Rangarajan S, Chilkoti A. Adv Maert. 2009; 21:2441–2446.
34. Lipka J, Smmler-Behnke M, Sperling RA, Wenk A, Takenaka S, Schleh C, Kissel T, Parak WJ, Kreyling WG. Biomaterials. 2010; 31:6574–6581. [PubMed: 20542560]
35. Kocbek P, Obermajer N, Cegnar M, Kos J, Kristl J. J Controlled Release. 2007; 120:18–26.
36. Acharya S, Dilnawaz F, Sahoo SK. Biomaterials. 2009; 30:5737–5750. [PubMed: 19631377]

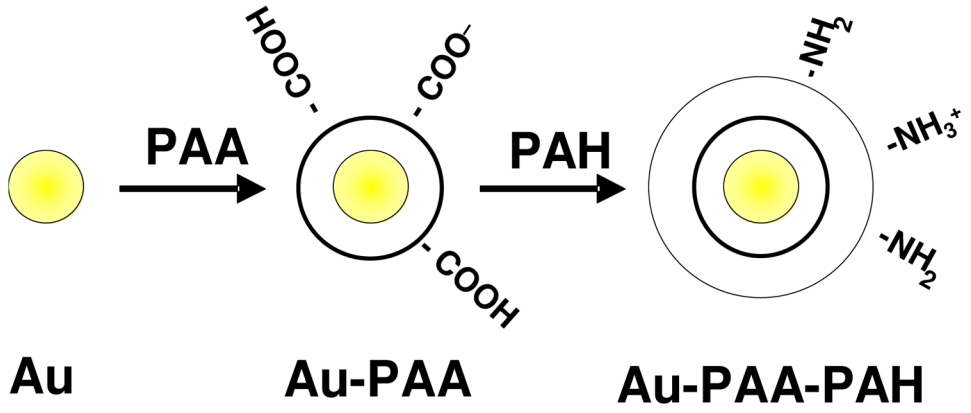

Figure 1.
Layer-by-layer polyelectrolyte coating of gold nanoparticles using anionic PAA and cationic PAH.

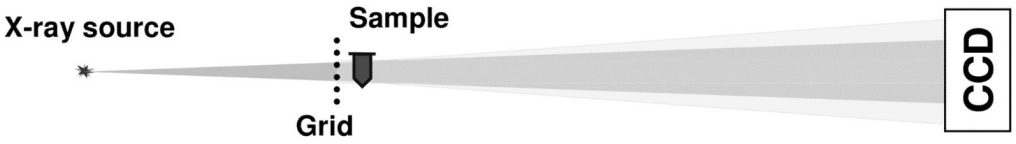

Figure 2.
Schematic of the x-ray imaging system.

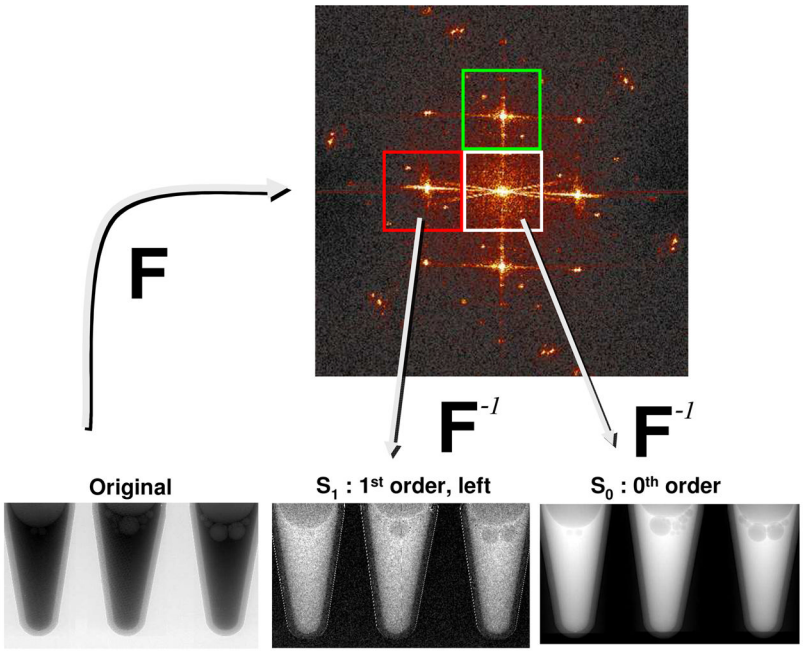

Figure 3.
Fourier transformation of an image with absorption grid and sample placed in the x-ray beam path gives an image in the spatial frequency domain. Different peaks in the spatial frequency image (surrounded by boxes) contain different information regarding how the sample scatters incident x-radiation.

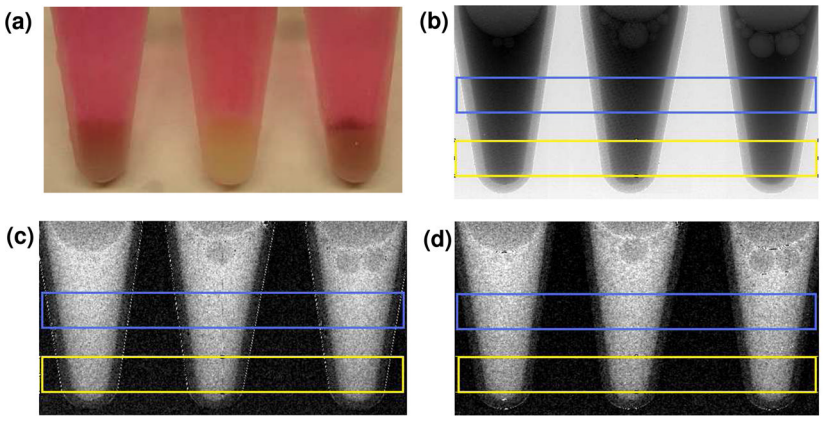

Figure 4.

Pellets of approximately 10^7 FOCUS cells labeled with 50 nm gold nanoparticles (left), no gold (middle), and 10 nm gold nanoparticles (right). Blue and yellow boxes indicate areas selected for intensity profiles of the supernatant and pellet, respectively. (a) Photograph of pellets under cell culture medium clearly shows gold labeling. (b) X-ray absorption image. (c) Left 1st-order processed image. (d) Upper 1st-order processed image.

Table 1

Cellular uptake of coated and uncoated gold nanoparticles.

	uncoated 10 nm AuNPs	10 nm Au-PAA-PAH	50 nm Au-PAA-PAH
mass of gold taken up per cell (pg)	1.2 ± 0.5	2.8 ± 0.4	2.2 ± 0.3
approximate number of nanoparticles per cell	108,000	275,000	1730
Approximate volume fraction of nanoparticles in each cell	0.00025%	0.00063%	0.00049%

Table 2

Average signal enhancements due to gold labeling.

		incubation 1	incubation 2
mass of gold taken up per cell (pg)		0.45 ± 0.09	0.76 ± 0.11
average number of nanoparticles per cell	10 nm	44,600	75,200
	50 nm	356	602
change in signal per pellet (%) [a]	original image	1.3 ± 4.4	1.1± 3.0
	processed image	1.6 ± 0.3	4.4 ± 0.8
signal enhancement per 1 pg of gold taken up per cell (%)	original image	2.9 ± 9.8	1.4 ± 3.9
	processed image	3.6 ± 0.7	5.7 ± 1.1
approximate potential signal enhancement for a pellet of 10^7 cells (%)		11 ± 2	17 ± 3

[a] All enhancements are reported in logarithm scale.